MRI on ion exchange resins at different length scales

Louis Kontschak[1] | Oliver Gruschke[2] | Lena Trapp[1] | Hatice Nur Baser[3] | Neil MacKinnon[3] | Philippe Rychen[4] | Hermann Nirschl[1] | Gisela Guthausen[1,5]

[1]MVM-VM, KIT, Karlsruhe, Germany
[2]Bruker BioSpin GmbH & Co. KG, Ettlingen, Germany
[3]IMT, KIT, Karlsruhe, Germany
[4]Ovivo Switzerland AG, Witterswil, Switzerland
[5]EBI-WCWT, KIT, Karlsruhe, Germany

Correspondence
Gisela Guthausen, MVM-VM, KIT, Karlsruhe, Germany.
Email: gisela.guthausen@kit.edu

Funding information
Deutsche Forschungsgemeinschaft

Abstract

Ion exchange resins were studied on different length scales by magnetic resonance imaging (MRI) with the focus on their interactions with nanoparticles (NP) and molecular clusters. On the length scale of resin beds (bed diameters <20 mm), the behavior of NP and of molecular clusters was shown to depend on the kind of ion exchange resin and nanoscale moiety. The kinetics of absorption and penetration into the resin beads was quantified on a smaller length scale of a stack of resin beads (sample with an outer diameter of 1.7 mm). Finally, using an MRI μ-coil (3D spatial resolution ≥8 μm), adsorption of superparamagnetic NP on individual resin beads was observed via the magnetic field disturbance characteristic for magnetic dipoles. As a result, this allows the detection of NP (diameter ≤100 nm) by MRI on much larger length scales of several micrometers.

KEYWORDS
absorption kinetics, contrast agents, ion exchange resins, MRI, superparamagnetic nanoparticles, μ-coil

1 INTRODUCTION

In our environment, nanoparticles (NP) play a considerable role in pollution, and thus their fate and behavior are of major interest. For example, microplastics are found almost everywhere, and strategies are needed for efficient detection and removal. Microfabrication, on the other hand, needs absolutely well-defined substances, one being water. Huge efforts are made to provide ultra-pure water for the semiconductor industry, where the microstructures are comparable in size with NP contaminants. Ion exchange via polymeric gel resins in the form of beads allows for the required cleaning. The fundamentals were published in Reichenberg,[1] the aspects related to environmental impact are summarized in Vagliasindi et al.,[2] and typical characterization methods can be found in Golden,[3] for example. Often, cationic and anionic resins are used with their specific exchange properties given by their chemistry. However, questions arise about their efficiency as absorbers. On the macroscopic scale, the distribution and dynamics of NP in the columns are of interest. The column filtration properties are usually characterized by the point of breakthrough as a function of operating conditions. The breakthrough is considered as measure of the column quality with respect to capacity,[4] for example, one indicator is the pH value.[5] The separation process, particularly on the mesoscopic scale, is the primary focus of this research using magnetic resonance imaging (MRI) on different length scales: is the separation dictated by steric properties of the packed beds, or does it start in the gores between the beads? Is the efficiency determined by nanoscale interactions between NP and resins leading to penetration? Can the kinetics—depending on the nanoscale moieties—be measured?

On the microscopic scale, the distribution of NP on/in a single resin bead is of interest. The relevant interactions and their strength need to be identified and quantified on that scale to gain an understanding of the macroscopically observed retention, breakthrough, and reversibility.

In-depth investigations need to be performed non-invasively and non-destructively—preferentially by imaging modalities. Requirements

Abbreviations: BNF, bionized nanoferrite; FLASH, fast low angle shot, pulse sequence; FOV, field of view; MRI, magnetic resonance imaging; NMR, nuclear magnetic resonance; NP, nanoparticles; PRE, paramagnetic relaxation enhancement; PW, pure water; RARE, rapid acquisition with relaxation enhancement, pulse sequence; rf, radio frequency; SPION, superparamagnetic iron oxide nanoparticle.

concern an adequate time resolution together with spatial resolution and image contrast in the optically opaque media. One analytical modality to be considered is MRI, for example,[6] where water and the resins as potential absorbers provide sufficient MR image contrast. Do the NP themselves generate sufficient contrast, and can they be detected on and in the resins with image resolutions of much larger length scales than their diameter? Are NP only spatially distributed along the hydrodynamic forces, are they attached at the resin surface, or do they penetrate into the resin beads? Are the nanoscale moieties still mobile in the context of retention, reversibility, and rinsing out? These questions are addressed by exploring the behavior of superparamagnetic NP and molecular cluster MRI contrast agents.

In more detail, MRI provides spatially resolved insight into non-metallic materials—independent of optical opaqueness. This is particularly significant in the fields of chemical engineering[7] and, more general, materials science,[8] where processes are often studied time-resolved via consecutive measurements. Examples are the study of heterogeneous catalysis[9] and membrane filtration regarding fouling[10] and wetting.[11] The image contrast is often based on nuclear magnetic resonance (NMR) relaxation properties, especially on transverse relaxation. These principles are applied in this work to study water purification using superparamagnetic NP (Fe_2O_3 and Gd_2O_3) and a molecular cluster-based medical MRI contrast agent (Magnevist). These substances differ in size, in surface charge, in relevant interactions with the resin's chemical substances, but also in their MRI properties. Both types of contrast agents cause paramagnetic relaxation enhancement (PRE), for example,[12] superparamagnetic NP mainly shorten the transverse relaxation T_2 and cause magnetic susceptibility-induced disturbance of the local magnetic field homogeneity,[13] thus altering the contrast in an image. Magnevist is regarded as a mainly T_1-reducing contrast agent in aqueous environments, which also yields a signal enhancement in a given measurement time.[14] However, it is well known that PRE relaxivities (relaxation divided by the contrast agent's concentration) depend not only on the properties of the moieties themselves,[15] but also on the properties of the environment. This becomes evident when looking at the theoretical description of PRE, where also rotational and diffusional correlation times enter the equations (e.g., Refs. 12,16–18), leading to material-specific performance of the MRI contrast agents.[19]

In this work, the different (super-)paramagnetic species were effectively used to study the ion exchange resins in detail. The MRI length scales spanned the millimeter to micrometer ranges, and the contrast agents revealed insight into time scales of penetration and adsorption as a function of resin and contrast agent chemistries. The MRI hardware, together with the experimental parameters and methods were established. Dedicated data treatment procedures were applied to deduce the parameters that characterize the processes.

2 MATERIALS AND METHODS

Three experimental approaches were realized to answer the questions about ad- or absorption, penetration, and the interaction of nanoscale moieties with the resins on mesoscopic and microscopic scales. First, the resin beads were placed in 10 / 20 mm glass tubes in pure water (PW). The volumes of the resin beads amounted to 0.5 and 1.6 mL, respectively. Aqueous contrast agents were added on top of the bed with the aim to gain insight into sedimentation and diffusion in the concentration gradient as well as into ad- / absorption of the contrast agents in the presence of the resins.

Second, a glass pipe with an outer diameter of 1.7 mm and an inner diameter of 0.7 mm was used to study the named processes on a smaller length scale with better MRI spatial resolution. Fluidic coupling allowed the control of fluid exchange from the outside of the magnet, avoiding repositioning of the sample and facilitating the quantitative study of penetration. In this case, the fluid was replaced from the bottom of the sample. A sufficiently good time resolution allowed for the spatially resolved observation and quantification of the penetration progress of the contrast agents into the resin beads.

Third, single resin beads were studied applying superparamagnetic NP. This study had the variety of interactions and forces in its focus.

2.1 Materials: resins and contrast agents

Ion exchange resins were provided by Ovivo Switzerland AG. Both anionic and cationic polymeric resins were available as nearly spherical beads with mean diameters in the range of 600 µm (corresponding to the optically measured mean diameter $2r_M$). The polymer polystyrene was chemically crosslinked by divinylbenzene (3%–6%). The resins were adapted to the specific purposes of anion or cation exchange via their functional groups: sulfonic acid in the case of strong acid cationic exchange resins (in the form of H) and quaternary ammonium for strong basic anionic exchange resins (in the form of OH). Their ion exchange capacity varies from 1.4 to 2.2 equivalent/L for strong basic anionic resins and strong acid cationic resins, respectively. The bulk densities of the resins are in the range of 0.7–0.8 g/cm^3.

The superparamagnetism of NP was exploited to image their deposition in the beds or at/in single beads of ion exchange resins by MRI. Diverse chemical compositions of superparamagnetic NP are known, while the coating of the NP and their size determine the interaction with the resins and therefore adsorption and penetration. In this study, a variety of contrast agents in the form of NP and a molecular cluster were explored to cover the range of possible interactions.

Well-known NP are those with a core of Fe_2O_3 fragments, which provide the superparamagnetism needed for the detection of the NP via PRE on the comparatively crude length scale of MRI. Please note that these NP mainly introduce negative image contrast due to the dominantly transverse PRE. The cohesion of Fe_2O_3 crystallites is realized by polymers like dextran or (poly)vinyl alcohol. These composites are additionally coated to provide application-specific chemical compatibility. In this work, Fe_2O_3 NP with SiO_2 and dextran coatings were used. The mean particle sizes were 52 nm (Silica@SPIONs, SiO_2 coated Fe_2O_3, zeta potential −41 ± 2 mV, BH2N Laboratoire Interdisciplinaire Carnot de Bourgogne, Dijon Cedex, France), and 80 nm

(BNF-dextran NP, dextran coated Fe_2O_3, zeta potential 7 ± 7 mV, micromod Rostock, Germany). All Fe_2O_3 NP are dominantly transverse relaxation enhancers, the transverse relaxivities are 6.8 L/(mg(Fe) × s) and 2.5 L/(mg(Fe) × s) measured at a ^{1}H Larmor frequency of 200 MHz.

Gadoluminate was purchased from Bio-PAL (MA, USA) and applied in the bed studies. Gadoluminate is a neutral gadolinium oxide colloid (Gd_3O_4 coated with dextran, zeta potential 4 ± 3 mV) with a mean diameter of 20–30 nm. It shows both T_1 and T_2 contrast in water due to the electronic correlation time of Gd^{3+} [18]: the relaxivities are $r_1 = 31–39\ L/(g \times s)$ and $r_2 = 61\ L/(g \times s)$ measured at 400 MHz.

The gadolinium cluster Magnevist (Gadopentetat-Dimeglumin, $C_{28}H_{54}GdN_5O_{20}$, molar mass: 938,00 g/mol) is a molecular cluster with Gd^{3+} as paramagnetic center. It was obtained from Bayer Vital GmbH (Germany) and was applied to study absorption/penetration into the resin beads. It is a predominantly T_1 contrast agent in water. Its smaller size facilitates penetration and was used to study the penetration kinetics in stacked beads in a glass pipe. The concentration was 0.6 mmol/L, and the complete water volume of 0.023 mL in the sample was exchanged via the fluidic coupling (Section 2.2.2).

2.2 Magnetic resonance imaging

One limiting fact in MRI results from the involved energy quanta. The energy of a nuclear spin transition is rather small, being the reason for the inherent insensitivity of NMR when compared, for example, with optical modalities. One attempt to reach the physical limit is to design the radio frequency (rf) circuit of the MRI, especially the transmit/receive coil, such that the signal-to-noise ratio is at its maximum for the question to be answered.

At larger length scales, bird-cage coils adequately fulfill this requirement. At small length scales, different coil geometries are used, and μ-coils are known to deliver better signal-to-noise due to the adaptation of the coil's geometry to the sample under consideration. Therefore, MRI experiments on stacks of resin particles and single resin beads exposed to NP were performed using a 1.7 mm coil[20] and a μ-coil[21] at a ^{1}H armor frequency of 400 MHz to improve sensitivity.

The MRI experiments were performed on an Avance HDIII 200 MHz super wide bore spectrometer and an Avance Neo spectrometer (Bruker BioSpin GmbH & Co. KG, Ettlingen, Germany) equipped with a wide bore 400 MHz magnet. Both spectrometers have imaging hardware (Great amplifiers 60 A, micro 2.5 and micro 5 gradients) and diverse rf probes. The software for experiment control and data acquisition was Paravision 6 and Paravision 360, respectively. The experimental parameters of all experiments are summarized in Table 1.

2.2.1 MRI studies on beds

Resin beds were measured at 200 MHz with a birdcage MICWB20 RES200 ^{1}H 040/020 QTR to study the behavior of the superparamagnetic NP in the resin bed. At 400 MHz, a quadrature micWB40 ^{1}H resonator with a 25 mm sample diameter (MICWB40 RES400 1H 040/025 QTR) was used to measure beds of ion exchange resins with Gadoluminate NP. The resin beads were filled into a conventional NMR tube with an outer diameter of 20 mm with a filling level of 25 mm. Fast low angle shot (FLASH) and rapid acquisition with relaxation enhancement (RARE) experiments were used with the parameters listed in Table 1.[22]

2.2.2 Hardware to study penetration kinetics

To study the absorption kinetics in detail, an rf coil insert for a maximum sample diameter of 1.7 mm was used, mounted on a Diff 30 probe equipped with a micro 5 MRI gradient allowing spatial resolution along *x*, *y*, and *z*. The dewar and the temperature control elements were removed from the probe, and the now available space was used for fluidic coupling to the sample. The glass tube was open on both sides and tapered on the bottom to retain the resin beads in the sensitive volume of the probe while water with contrast agents can pass. As in the case of experiments on beds, the RARE pulse sequence was applied with the parameters in Table 1. During the dynamic experiments, T_R was 2.5 s for better time resolution, while

TABLE 1 Experimental parameters of the magnetic resonance imaging (MRI) experiments, listed as a function of samples and the studies purposes.

MRI parameters for measurements on:	Bed (200 MHz, 20 mm birdcage)	Bed (400 MHz, 20 mm birdcage)	Stack of beads (1.7 mm coil)	Single bead (μ-coil)
MRI pulse sequence	FLASH	RARE	RARE	RARE/FLASH
Recycling delay T_R	0.5 / 0.7 s	2.5 / 3 s	8 / 5 / 2.5 s	0.25 / 0.1 s
Echo time τ_E	3 / 4.2 ms	13 / 7.5 ms	2.76 ms	2.58 / 0.02 ms
RARE factor		17 / 4	11	1
Digital matrix size	256 × 256	512 × 512	128 × 128	100 × 100
Field of view (FOV)	15 mm × 15 mm	20 mm × 20 mm	1.7 mm × 3.4 mm	1.5 mm × 1.5 mm
Pixel size	59 μm × 59 μm	39 μm × 39 μm	13 μm × 27 μm	15 μm × 15 μm
Slice thickness	0.5 mm	0.4 mm	0.2 mm	0.13/0.1 mm

Abbreviations: FLASH, fast low angle shot; RARE, rapid acquisition with relaxation enhancement.

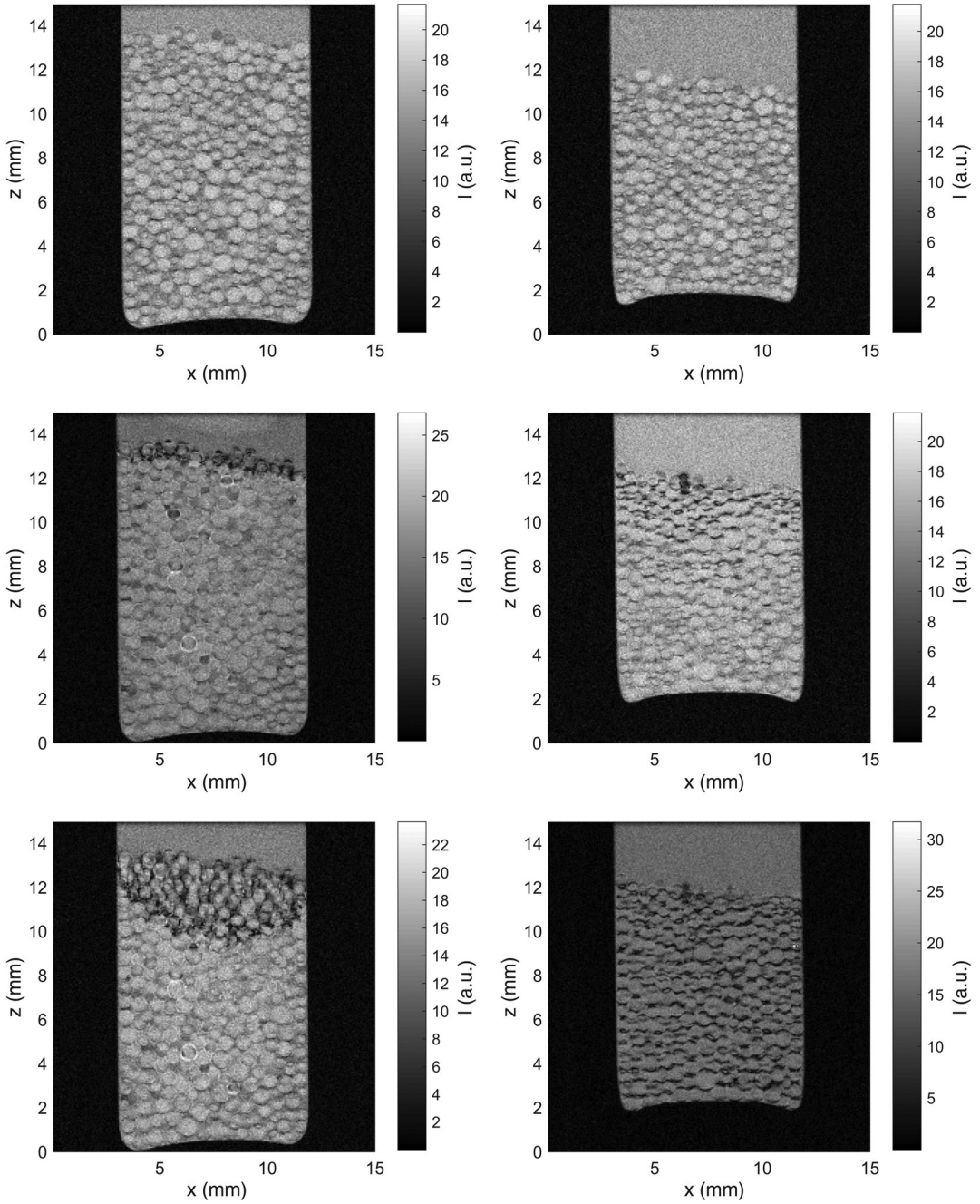

FIGURE 1 Beds of anionic ion exchange resins measured via sagittal MRI slices in the middle of the bed (top: References without NP). Two-dimensional images are shown with the NMR intensity *I* on the indicated false color scale. Left: The bed was exposed to bionized BNF-dextran NP for 1 h 54 min (middle) and 18 h 43 min (bottom), a progressing of a front is evident. Right: Silica@SPIONs NP were added on top of the bed and measured after a contact time of 2 h 32 min (middle) and 17 h 37 min (bottom). While the image contrast changes, no clear progression front, but a diffuse behavior was observed.

$T_R = 5$ s and 8 s was used before the injection of the contrast agent and at the end for measuring the equilibrium states with good signal-to-noise ratio.

2.2.3 μ-Coil setup for minimal spatial resolution

For spatial resolution down to 8 μm, a Helmholtz μ-coil was used to study a single resin bead (^{1}H 400 MHz MICLAB400 ^{1}H HELM1000AM VS1). Paired with the micro 5 gradient and Diff30 probe base, the μ-coil enables investigating samples with a maximum thickness of 500 μm and with a sensitive plane of up to 1 mm × 1 mm. The single resin bead was placed inside an acrylic glass sample holder in a cavity filled with PW with or without contrast agents. A PCR film sealed the cavity and prevented the bead from moving. The sample holder was inserted into the μ-coil and aligned to ensure that the bead was in the center of the sensitive volume. In-plane digital resolution was 15 μm × 15 μm (Table 1).

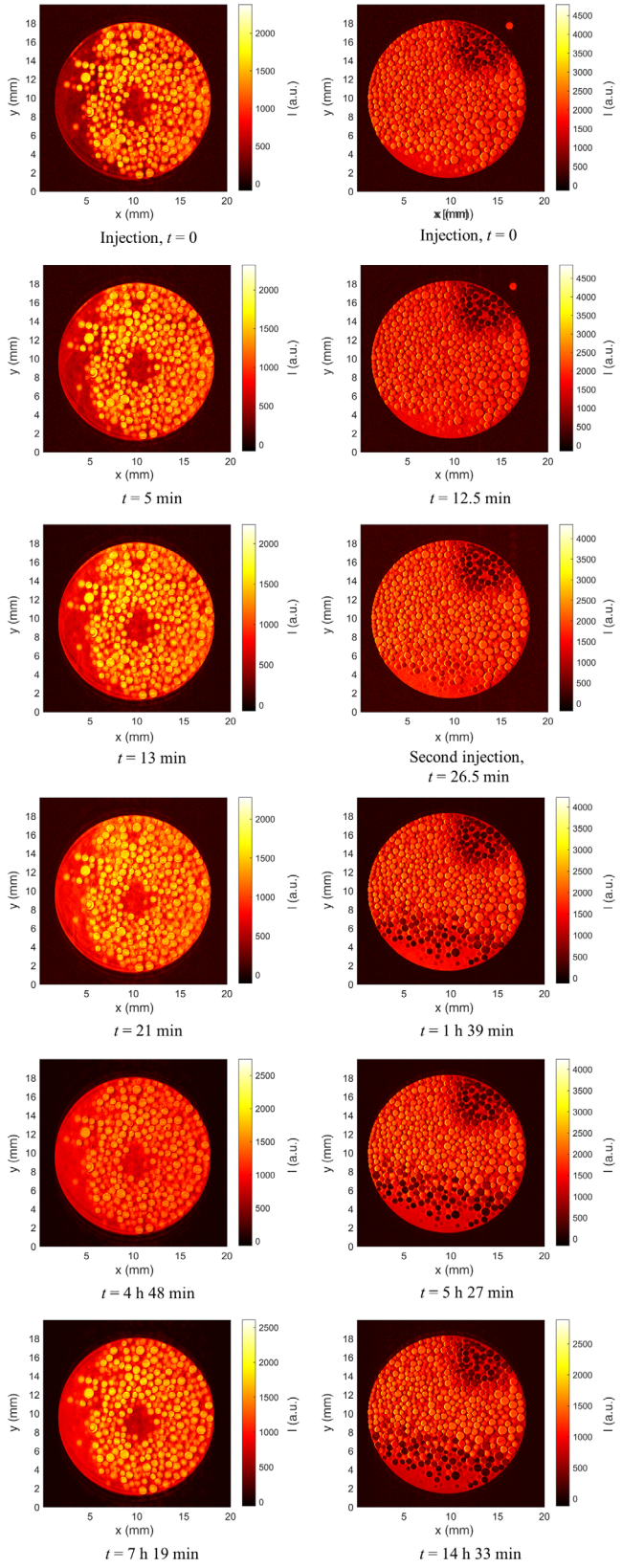

FIGURE 2 Interaction of neutral Gadoluminate NP in beds of anionic (left) and cationic (right) resin beads. The implicit parameter is the time after injection. While in an anionic resin bed (left), sedimentation through the measured slice is observed; penetration and absorption of Gadoluminate particles into the cationic resin beads is obvious (right).

2.3 Data processing

Apart from data processing within Paravision (Fourier transform, magnitude calculation, super resolution), data were processed by self-written MATLAB scripts for image presentation and deduction of process parameters. The latter was done by exploiting the spherical geometry of the resin beads. The signal amplitude differs significantly between resin and aqueous environment, allowing for the application of the ring method. This image processing tool was originally developed for observing fouling in hollow fiber membrane filtration, first of alginate[23] and second of skim milk.[10] The interesting section of an image is masked, exploiting the mentioned difference in signal amplitude, and rings are then selected with decreasing diameter. The intensities within a ring are averaged over the angle, leading to an intensity profile along the radial coordinate of the object. Under the prerequisites of circular geometry in the image and sufficiently small slice thickness compared to the beads size (i.e., the neglection of partial volume effects is possible), this numerical data reduction reveals the radial profiles of contrast agents in the resin beads as a function of time. Modeling of these profiles leads to the quantification of absorption/penetration of the contrast agents.

3 RESULTS AND DISCUSSION

3.1 Nanoparticles in packed beds of ion exchange resins

Questions about deposition, fate, and behavior of NP in beds of ion exchange resins were addressed. In a first experiment at 200 MHz ^{1}H Larmor frequency, the resin beads were exposed to the technically more relevant Fe_2O_3 NP (BNF-dextran and Silica@SPIONs) on top of the bed, while sagittal MR images were acquired.[24] The droplet of the NP suspension dilutes in the bed's PW, and the NP start to sediment. However, the left and right rows in Figure 1 show that the behavior of the two kinds of NP differs: while a clear front was observed for the BNF-dextran NP with a rather long-time course, Silica@SPIONs NP spread out and were preferentially found on top of the resin beads in the bed's gores due to the geometric hindrance by the resin beads, thus playing a major role during sedimentation.

The interaction of the NP with the resins differs—BNF-dextran NP interact, while Silica@SPIONs sediment—due to the specific surface chemistry of the NP. The crude distribution of both types NP in the bed is visible, allowing the differentiation of sedimentation and interaction. However, penetration or adsorption are hardly distinguishable in these experiments at 200 MHz. The spatial resolution is not sufficiently good, but susceptibility artifacts do not hamper the overall detection of the superparamagnetic particles in the packed bed of ion exchange resin beads. Questions remain about the exact location of NP in the beds and the details of interactions between NP and resin.

In a second experiment, the behavior was observed in axial slices when loading cationic and anionic resin beds with a droplet of an aqueous Gadoluminate suspension, measured at 400 MHz ^{1}H Larmor

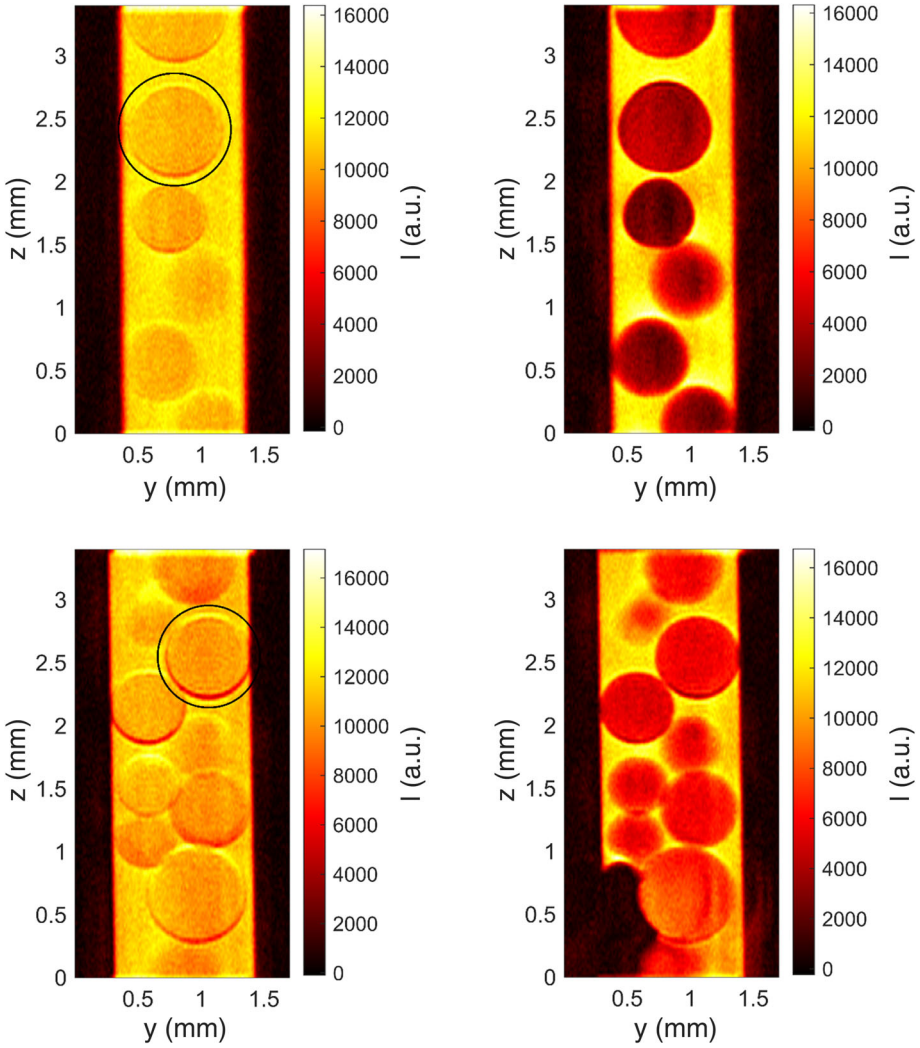

FIGURE 3 Top: Anionic resin beads in water (left) and Magnevist solution after 1.5 h (right). Bottom: Cationic resin beads in water (left) and Magnevist solution after 1 h (right). In the rather similar images of the resins in water, the bead is indicated for which the penetration kinetics was deduced. The penetration of the contrast agent is obvious in the final images on the right, leading to reduced signal intensity in the resins.

frequency. Gadoluminate offers mixed R_1 and R_2 MR image contrast, while the mean particle size is still in the same order of magnitude as for the Fe_2O_3 NP. A droplet was put on top of the beds of anionic and cationic beads. Concentration equilibration, sedimentation, and ad- and absorption were measured via multiaxial slice imaging as a function of time after injection.

Axial RARE images are shown (Figure 2), which are less sensitive to susceptibility differences than FLASH, as RARE relies on transverse relaxation T_2 and not on the effective T_2^*.[22] This is even more important for measurements at 400 MHz compared to the previously discussed 200 MHz ^{1}H Larmor frequency, as the influence of magnetic susceptibility scales with the magnetic field. A slice near the aqueous supernatant on top of the beds is shown, providing direct insight into both sedimentation and absorption of NP. In the first case, the Gadoluminate NP penetrate the bed and are distributed over the bed's volume (Figure 2, left). The time course shows the appearance and disappearance of Gadoluminate via transverse PRE, reflected by regions of decreased signal intensity in the regions of higher Gadoluminate concentration. The transverse PRE-induced reduction of intensity disappears with time, as the NP distribute and sediment. At later times, the images show larger and fairly homogeneous signal intensities in the water phase and in the resin beads.

The interaction between cationic resin and Gadoluminate differs significantly (Figure 2, right): a first droplet was injected, and the NP are absorbed within the measurement time (dark area x >10 mm, y >13 mm). Again, the image contrast was increased by transverse PRE. The penetration kinetics is therefore fast and below the measurement time of approximately 6 min. The absorption is stable in time, and the NP distribution from the first injection remains unchanged after the injection of a second droplet (y <6 mm, t = 26.5 min). As with the first injection, absorption is once again fast, and the distribution is constant over time, leading to the conclusion that the state of absorption is thermodynamically favored.

3.2 Absorption of contrast agents in stacked ion exchange resins

The MRI measurements so far showed the behavior of nanoparticulate substances in packed beds of ion exchange resin beads, ranging from adsorption/penetration to no interaction/sedimentation.[25] The mean

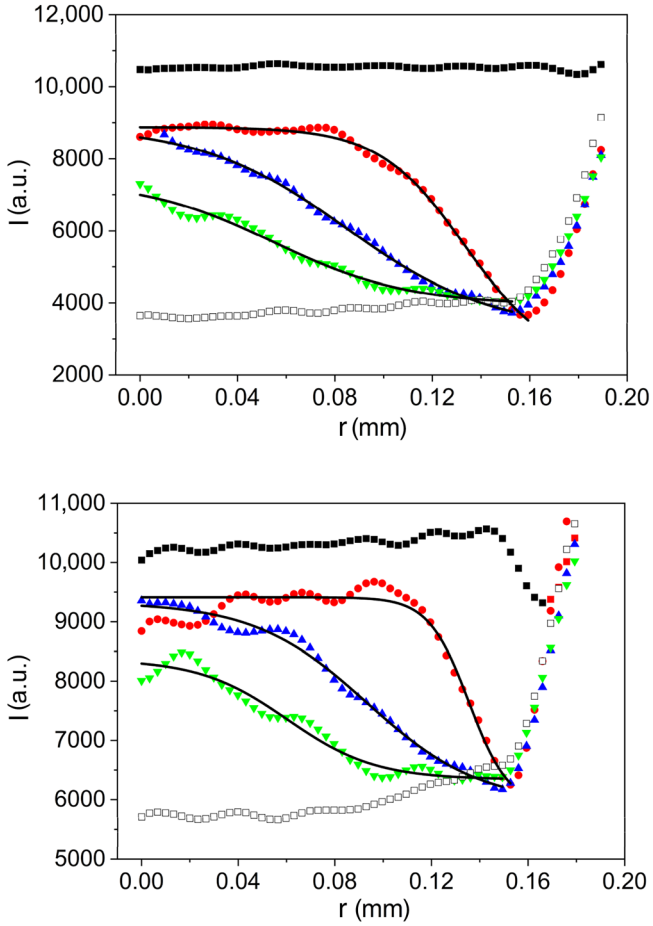

FIGURE 4 Top: MRI signal intensity I, averaged over the angle (0 … 2π) as a function of the radial coordinate of the selected anionic resin bead (Figure 3). The symbols indicate times during the penetration process (■: resin in PW, ●: after 4 min of injection of the aqueous Magnevist solution, ▲: after 8 min, ▼: after 12 min, □: after 1.5 h), bottom: cationic resin at the following times: ■: resin in PW, ●: after 3 min of injection of the aqueous Magnevist solution, ▲: after 7 min, ▼: after 11 min, □: after 1 h). The solid lines correspond to sigmoidal modeling.

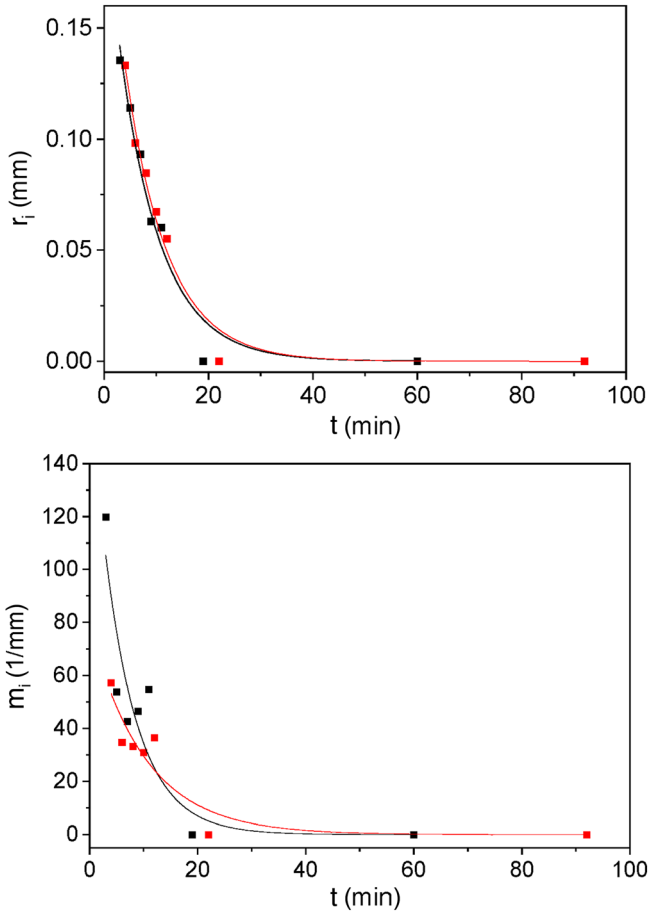

FIGURE 5 Inflection point (r_i, top) and slope at the inflection point (m_i, bottom) as a function of exposure time t for anionic (red) and cationic (black) resins together with the modeling by an exponential decay (solid line).

sizes of the NP were between 20 and 80 nm, and the question arises whether size, surface charge, or specific chemical interactions play a major role. The nanoscale moieties were therefore varied: Magnevist as a molecular cluster offers the possibility to study the behavior on an order of magnitude smaller length scale (range of 1–2 nm). To improve the MRI spatial resolution, a glass pipe in a 1.7 mm coil was used, which contained the resin beads, and MRI measurements (Table 1) were performed as a function of time after injection of aqueous contrast agent for both anionic and cationic resins (Figure 3). The images show a reduced signal intensity of the beads when Magnevist was absorbed, which is more pronounced for the anionic resins. A positive image contrast is expected for Magnevist as a preferentially R_1 contrast agent in water. The observation in Figure 3 indicates that the rotational and diffusional correlation times of the contrast agent changed in the polymer matrix of the beads, leading to increased transverse relaxivities.

The echo time was short (2.76 ms, Table 1), even then, the effect was observed. In addition, it should be mentioned that the images of resins in water show a pronounced susceptibility artifact along the read direction (z), which of course influences the quantification mainly at the edges via the ring method.

For both, anionic and cationic resins, one bead was selected for quantification of the kinetics (Figure 3, circles). Using the ring method (Section 2.3), the signal intensities, averaged over the angle at a given radial distance, were extracted from the images recorded during the penetration of the small molecular clusters into the resins (Figure 4). It is worth noting that the images at the beginning were recorded with a repetition time of 8 s. The repetition time was changed from 2.5 s during the process to 8 s (anionic) and 5 s (cationic) for the last measurements. Therefore, the absolute intensities reflect the magnetization attenuation due to the smaller repetition time rather than the penetration of Magnevist into the beads, such that the radial dependence of the intensity is analyzed rather than the absolute intensities.

The intensities were modeled by a sigmoidal function:

$$I(r,t) = (I(r \to \infty, t) \quad I(0,t)) \left(1 \quad \frac{1}{1 + \exp(m_i(t)(r \quad r_i(t)))}\right) + I(0,t),$$

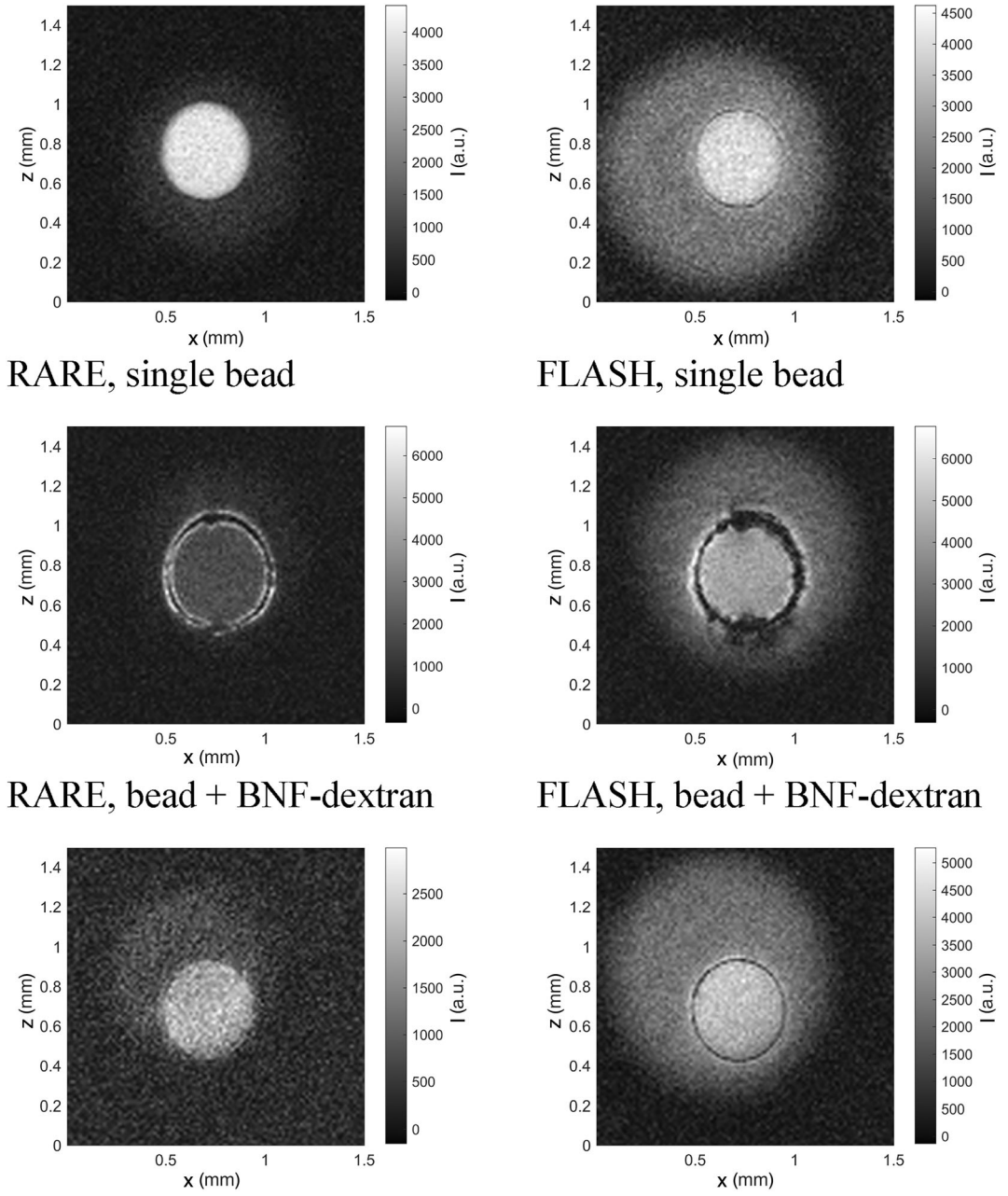

FIGURE 6 μ-MR images on single resin beads exposed to nanoparticles (NP): ***anionic*** resin beads without exposure (top), and exposed to BNF-dextran NP (middle) and Silica@SPOINs (bottom). Left: RARE images, right: FLASH images, for illustrating the importance of magnetic susceptibility on the small length scale of a μ-coil at 400 MHz.

where $r \to \infty$ indicates the outside of the resin bead. The most meaningful fit parameters are the inflection point r_i and the slope at that inflection point m_i. The signal intensity at $I(r = 0, t \to \infty)$ reflects the relaxivities of Magnevist in the resin times the equilibrium concentration at a given T_R. Important parameters in the observation of the penetration kinetics are $r_i(t)$ and $m_i(t)$, that is, the time-dependent inflection point and the corresponding slope (Figure 5). These parameters are sensitive to the relative concentration gradients within the resin beads. Both can be described by an exponential decay, leading to a time constant of 8 ± 1 min for $r_i(t)$ for both anionic and cationic resins, and $m_i(t)$ of 10 ± 3 min (anionic resin) and 6 ± 2 min (cationic) results. The penetration of the small molecular clusters Magnevist into the resin beads is thus measurable by MRI with subsequent image processing, and its kinetics is on the order of 8 min within the experimental error. It is worth noting that PRE of Magnevist in the beads differs from PW state. In PW, PRE is mainly R_1, a combined R_1 and R_2 PRE is observed in the resins (Figure 3, right).

3.3 Single resin beads: penetration of contrast agents

As the images measured on the beds (Figure 1) are limited in the spatial resolution, the behavior of the Fe_2O_3-based NP needs to

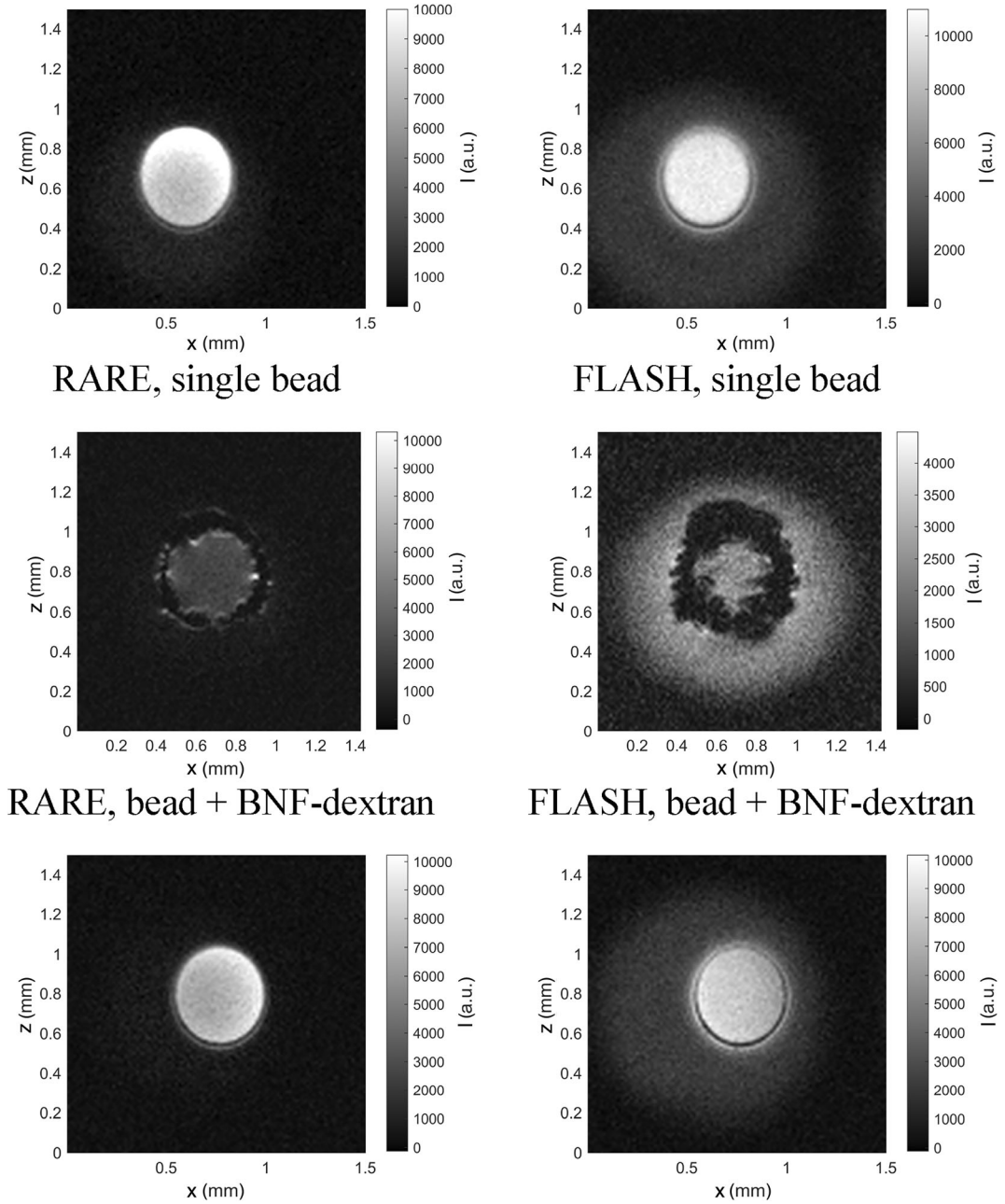

FIGURE 7 μ-MR images on single resin beads exposed to nanoparticles (NP): ***cationic*** resin beads without exposure (top), and exposed to BNF-dextran NP (middle) and Silica@SPIONs NP (bottom). Left: RARE images; right: FLASH images: BNF-dextran NP are more pronounced adsorbed to cationic resins, while Silica@SPIONs NP show less effects in the images.

be studied in more detail regarding their adsorption on or penetration into the resin beads.[26] This aspect of the study was addressed in experiments on single beads. Localization of the superparamagnetic NP on and in the resin beads can thus be studied by observing a single resin bead exposed to the contrast agents (Figures 6 and 7). A very good spatial resolution can be achieved for that purpose with a μ-coil. Anionic and cationic resins were exposed to BNF-dextran and Silica@SPIONs NP. The images show the specific interactions between the materials measured as well as with the NMR static magnetic field (400 MHz, 9.4 T). The pulse sequences RARE / FLASH have their specific view on the materials, especially concerning magnetic susceptibility and relaxation ($T_{1,2}$ and T_2^*) contrast. The dependence on the refocusing properties of the pulses becomes evident (Figures 6 and 7), for explanations, we refer to, for example, Callaghan.[22] The images as such already provide insight into the behavior of the superparamagnetic NP in the magnetic field and in the neighborhood of the resins. Further quantification was done by the ring method of angular averaging, which provides the distribution of NP nearby and in the resin beads.

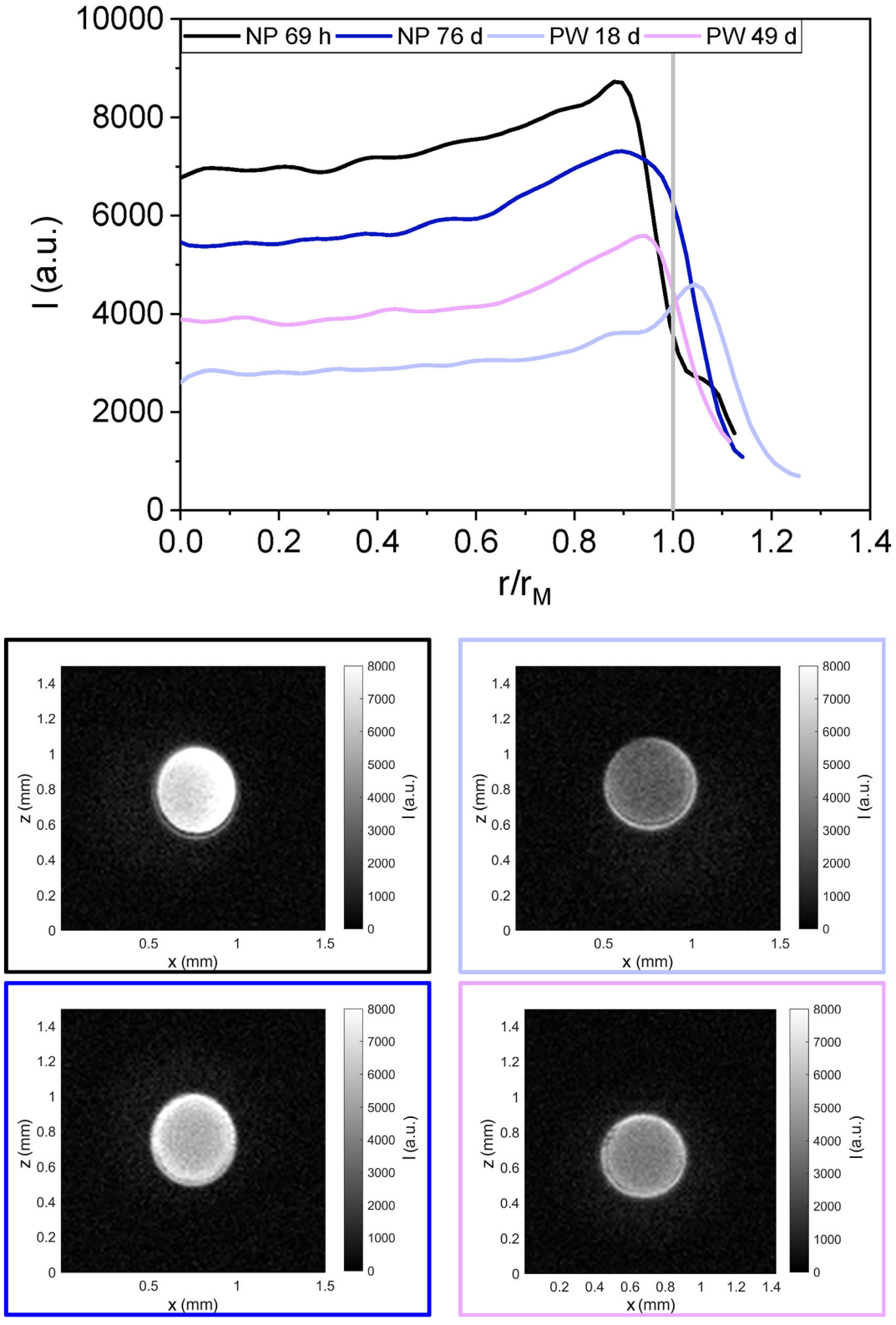

FIGURE 8 μ-MRI on cationic resin beads, exposed to Silica@SPIONs NP (NP, duration) and afterwards exposed to pure water (PW, duration). Evidence for penetration is given for small values of r/r_M (black and dark blue lines and images) as well as for back-diffusion on long-time scales (light blue and purple). The gray mark corresponds to the optically measured bead radius r_M.

The μ-MR images of both resins without exposure to PRE-causing moieties show the bright interior of the beads together with susceptibility-induced artifacts at the particle edge caused by the susceptibility difference between the polymer and surrounding water. In the presence of BNF-dextran NP, the situation changes: while both sequences show an adsorption of the NP on the anionic resin, the MR images of the cationic resin bead to BNF-dextran NP are significantly disturbed by the superparamagnetism of the BNF-dextran particles. In the case of Silica@SPIONs, with roughly one third of transverse relaxivity, no apparent signature in the images was observed. This leads to the conclusion that—supported by the findings in Figure 1—the interaction of both resins with this type of NP is weak, either no or a homogeneous penetration is detected on the time scale of the exposure. Figure 8 provides the quantification: The ring method allows the determination of the angularly averaged intensity as a function of exposure to NP and rinsing time (exposure to PW), respectively. The intensity within the bead is almost constant ($r < 0.7\ r_M$), while its absolute value depends on the exposure and the rinsing time. This indicates that the NP diffuse into the resin bead and back to the surrounding PW phase, depending on the concentration gradient. In a next step, single particles were measured in flow-through mode, also revealing the discussed phenomena of adsorption and penetration.[27]

4 CONCLUSIONS

MRI revealed spatially and time-resolved insight into the interactions between particulate and molecular contrast agents and ion exchange resins. The study provides tools in form of MRI methods to answer questions regarding the microscopic interaction between the nanoscale moieties and the resins. Different length scales were explored: first, the scale of a model column (diameter of 8–17 mm); second, the scale of stacked resin beads (on the scale of 700 μm), and third the scale of a single resin bead (600 μm). This closer look into the single resin bead behavior was achieved by taking advantage of the improved sensitivity for small samples offered by μ-coils, leading to a better spatial resolution. (Super-)paramagnetic NP were used, which generate susceptibility differences as well as mainly transverse relaxation enhancement. Both mechanisms provide sufficiently good contrast in the MRI images. In addition to the nanoparticulate contrast agents with predominantly transverse relaxation enhancement, Magnevist, a medical contrast agent in the form of a molecular cluster on the nm scale, allowed to study penetration kinetics quantitatively, which was observed in stacks of resin beads. The time scale of kinetics was in a similar order of magnitude (≈8 min) for penetration of Magnevist into anionic and cationic resins.

NOMENCLATURE

FOV	field of view (mm × mm)
I	signal intensity (a.u.)
m_i	slope at the inflection point (a.u./mm)
r	radial coordinate (mm)
r_M	bead radius (mm)
r_i	inflection point (mm)
r_1	longitudinal relaxivity (L/g × s)
r_2	transverse relaxivity (L/g × s)
T_R	recycling delay (s)
T_1	longitudinal relaxation time (s)
T_2	transverse relaxation time (s)
T_2^*	effective transverse relaxation time (s)
t	ad- and absorption time (min)
τ_E	echo time (ms)

AUTHOR CONTRIBUTIONS

Louis Kontschak: Investigation; data curation; visualization, writing—original draft and review and editing. **Oliver Gruschke**: Conceptualization; hardware development; writing—original draft and review and editing. **Lena Trapp**: Investigation; writing—original draft and review and editing. **Hatice Nur Baser**: Writing—review and editing. **Neil MacKinnon**: Funding acquisition; supervision; writing—review and editing. **Philippe Rychen:** Funding acquisition; supervision; project administration; writing—review and editing. **Hermann Nirschl**: Resources; writing—review and editing; funding acquisition; supervision. **Gisela Guthausen**: Conceptualization; writing—original draft and review and editing; project administration; funding acquisition; supervision.

ACKNOWLEDGMENTS

The authors highly appreciate the work of K. Kopania, E. Mayrose, F. Sinaga, L. Klammsteiner during their master thesis within Pro^{2}NMR at MVM-VM, KIT. Technical assistance was given by S. Margiotta-Neu, additionally, valuable discussions are highly acknowledged with present and former members of the working group and industrial partners. Fruitful discussions and exchange with Ovivo personnel are highly appreciated. The authors would like to thank Deutsche Forschungsgemeinschaft DFG for financial support within the instrumental facility Pro^{2}NMR, especially for the instrumentation, ad within a "Sachbeihilfe" project, and within the Collaborative Research Center CRC 1527 Hyperion.

FUNDING INFORMATION

This work is supported by DFG, instrumental facility Pro^{2}NMR and CRC 1527 Hyperion.

CONFLICT OF INTEREST STATEMENT

The authors declare no conflicts of interest.

DATA AVAILABILITY STATEMENT

The numerical data and regression parameters underlying Figures 4 and 5 are available in Supporting Information S1 and S2.

ORCID

Louis Kontschak https://orcid.org/0009-0009-8855-7500

REFERENCES

1. Reichenberg D. Properties of ion-exchange resins in relation to their structure. III. Kinetics of exchange. *J Am Chem Soc*. 1953;75:589-597. doi:10.1021/ja01099a022

2. Vagliasindi FGA, Belgiorno V, Napoli RMA. Water treatment in remote and rural areas: a conceptual screening protocol for appropriate POU/POE technologies. In: Gavasci R, Zandaryaa S, eds. *Environmental Engineering and Renewable Energy*. Elsevier Science; 1998: 329-336.
3. Golden LS. Ion exchange resins: characterization. In: Wilson ID, ed. *Encyclopedia of Separation Science*. Academic Press; 2000:3172-3179.
4. Lee IH, Kuan Y-C, Chern J-M. Prediction of ion-exchange column breakthrough curves by constant-pattern wave approach. *J Hazard Mater*. 2008;152:241-249. doi:10.1016/j.jhazmat.2007.06.098
5. Harries R. Ion exchange kinetics in ultra pure water systems. *J Chem Technol Biotechnol*. 2007;51:437-447. doi:10.1002/jctb.280510402
6. Wallner AS, Ritchey WM. Applications of magnetic resonance imaging to ion-exchange resins. *J Appl Polym Sci*. 1995;57:1-6. doi:10.1002/app.1995.070570101
7. Gladden LF. Magnetic resonance in reaction engineering: beyond spectroscopy. *Curr Opin Chem Eng*. 2013;2:331-337.
8. Gladden LF, Sederman AJ. Magnetic resonance imaging and velocity mapping in chemical engineering applications. *Annu Rev Chem Biomol Eng*. 2017;8:227-247. doi:10.1146/annurev-chembioeng-061114-123222
9. Gladden LF, Abegao FJR, Dunckley CP, Holland DJ, Sankey MH, Sederman AJ. MRI: operando measurements of temperature, hydrodynamics and local reaction rate in a heterogeneous catalytic reactor. *Catal Today*. 2009;155:157-163. doi:10.1016/j.cattod.2009.10.012
10. Schork N, Schuhmann S, Nirschl H, Guthausen G. In situ measurement of deposit layer formation during skim milk filtration by MRI. *Magn Reson Chem*. 2019;57:738-748. doi:10.1002/mrc.4826
11. Wypysek D, Kalde AM, Pradellok F, Wessling M. In-situ investigation of wetting patterns in polymeric multibore membranes via magnetic resonance imaging. *J Membr Sci*. 2021;622:119026. doi:10.1016/j.memsci.2020.119026
12. Bertini I, Luchinat C, Parigi G. *Solution NMR of Paramagnetic Molecules: Applications to Metallobiomolecules and Models*. Vol 2. 1st ed. Elsevier Science B.V.; 2001.
13. Laurent S, Henoumont C, Stanicki D, et al. *MRI Contrast Agents: From Molecules to Particles*. Springer; 2016.
14. Powell DH, Dhubhghaill OMN, Pubanz D, et al. Structural and dynamic parameters obtained from ^{17}O NMR, EPR, and NMRD studies of monomeric and dimeric Gd^{3+} complexes of interest in magnetic resonance imaging: an integrated and theoretically self-consistent approach. *J Am Chem Soc*. 1996;118:9333-9346. doi:10.1021/ja961743g
15. Koenig SH, Brown RD. Field-cycling relaxometry of protein solutions and tissue – implications for MRI. *Prog Nucl Magn Reson Spectrosc*. 1990;22:487-567.
16. Vander Elst L, Roch A, Gillis P, et al. Dy-DTPA derivatives as relaxation agents for very high field MRI: the beneficial effect of slow water exchange on the transverse relaxivities. *Magn Reson Med*. 2002;47:1121-1130. doi:10.1002/Mrm.10163
17. Bertini I, Capozzi F, Luchinat C, Nicastro G, Xia ZC. Water proton relaxation for some lanthanide aqua ions in solution. *J Phys Chem*. 1993;97:6351-6354. doi:10.1021/J100126a007
18. Bertini I, Luchinat C, Parigi G, Ravera E. *NMR of Paramagnetic Molecules – Applications to Metallobiomolecules and Models*. Elsevier; 2017.
19. Schork N, Ibrahim M, Baksi A, Krämer S, Powell AK, Guthausen G. NMR relaxivities of paramagnetic, ultra-high spin heterometallic clusters within polyoxometalate matrix as a function of solvent and metal ion. *ChemPhysChem*. 2022;23:e202200215.
20. Bruker. Micro5. Accessed Sptember 20, 2024. https://www.bruker.com/en/products-and-solutions/mr/nmr/mr-microscopy-diffusion/mr-microscopy-probes/micro5.html
21. Bruker. Fruit fly meets microcoils – a magnetic resonance microscopy investigation of Drosophilae. Accessed September 20, 2024. https://www.bruker.com/en/products-and-solutions/mr/nmr/mr-microscopy-diffusion/mr-microscopy-probes/micro5/_jcr_content/root/contentpar/standardteaser/items/_33_1622530455788_co.download-asset.pdf/link/Fruit%20Fly%20Meets%20Microcoils%20-%20Application%20Note.pdf
22. Callaghan PT. *Principles of Nuclear Magnetic Resonance Microscopy*. Oxford University Press; 1991.
23. Schuhmann S, Schork N, Beller K, Nirschl H, Oerther T, Guthausen G. In-situ characterization of deposits in ceramic hollow fiber membranes by compressed sensing RARE-MRI. *AIChE J*. 2018;64:4039-4046. doi:10.1002/aic.16201
24. Herrling MP, Rychen P, Kopania K, Guthausen G. Ion exchange resins for advanced removal of nanoparticles from UPW? A novel imaging approach. Paper presented at Proceedings of the Ultra Pure Micro Conference 2019. 2019.
25. Klammsteiner L, Iyengar P, Herrling MP, Rychen P, Guthausen G. Interaction of nanoparticles with ion exchange resin beds in UPW polish systems. Paper presented at Proceedings of the Ultra Pure Micro Conference 2023. 2023.
26. Herrling MP, Rychen P, Guthausen G. Can nanoparticles penetrate UPW polishing resins? Nanoscale particle interactions by high resolution imaging of single resin beads. Paper presented at Proceedings of the Ultra Pure Micro Conference. 2020.
27. Herrling MP, Rychen P, Sinaga F, Schork N, Guthausen G. Nanoparticle adsorption of Polish IEX resins investigated by MRI. Paper presented at Proceedings of the Ultra Pure Micro Conference 2021. 2021.